INVESTIGATIONS ON CRACKS IN EMBEDDED SOLAR CELLS AFTER THERMAL AND MECHANICAL LOADING

Martin Sander[1], Sascha Dietrich[1], Matthias Pander[1], Matthias Ebert[1], Sven Thormann[2], Johannes Wendt[2] and Jörg Bagdahn[1,3]
[1]Fraunhofer Center for Silicon Photovoltaics, Walter-Hülse-Str. 1, 06120 Halle, Germany
[2] Q-Cells SE, Sonnenallee 17-21, 06766 Bitterfeld-Wolfen, Germany
[3]Anhalt University of Applied Sciences, Photovoltaic Materials, Bernburger Str. 57, 06366 Köthen, Germany

ABSTRACT: Cracks in crystalline solar cells in photovoltaic modules can be caused by applied mechanical stresses. To investigate the development of cracks in encapsulated solar cells a new approach was chosen that analyzes thermal and mechanical loading systematically. For this purpose two experiments are established using mini-module specimens with three or 10 cells. It was found by using electroluminescence imaging that after thermal loading small cracks (< 10 mm) were initiated mainly at the beginning and at the end of the busbars. After mechanical loading the cells show complete failure. The crack directions depend on the loading direction. Furthermore it was shown that a loading parallel to the busbars causes cracks at lower load magnitudes than a loading perpendicular to the busbars.
The findings can be transferred to full-scale modules by using finite element simulation results. The comparison with other investigations allows an interpretation of many effects that were observed in full-scale PV modules and allows design optimization for reduced cell breakage rates.
Keywords: Electroluminescence, Module, Cracks, Encapsulation, Reliability

1 INTRODUCTION

Photovoltaic modules (PV modules) are supposed to have a lifetime of more than 20 years under various environmental conditions like temperature changes, wind, snow, etc. Therefore cracks in encapsulated solar cells caused by thermal and mechanical loads play an important role, because they influence directly the electrical performance of the whole PV module [1-3]. These cracks are mostly invisible for optical inspection (naked eye) but can be identified using electroluminescence (EL) [4] and they can lead to isolated cell areas, thus causing reduced power output of the module [5, 6].

According to IEC 61215 full-scale PV modules are tested mechanically by applying a uniform area load on the horizontally mounted PV module. The cells are placed at the bottom side of the module and are connected to the glass via the encapsulant. Under pressure load tension stress from the bottom side of the glass is transferred to the cells via the encapsulant as shown by Dietrich et al. [7].

Typically after this mechanical load test several cells of the PV modules show a characteristic crack pattern that corresponds with observations on PV modules in the field, too. These characteristic crack directions can be found for both mono-crystalline and multi-crystalline cells.

The crack orientation in the cells and the spatial distribution of cracks in the module varies over the cell position [8, 9]. This indicates a non-uniform stress distribution and different stress directions in individual cells in the PV module under mechanical loading.

To get more information about the mechanics of crack development and crack growth in encapsulated solar cells an approach is chosen that investigates the crack formations systematically by testing mini-modules under well-known boundary conditions.

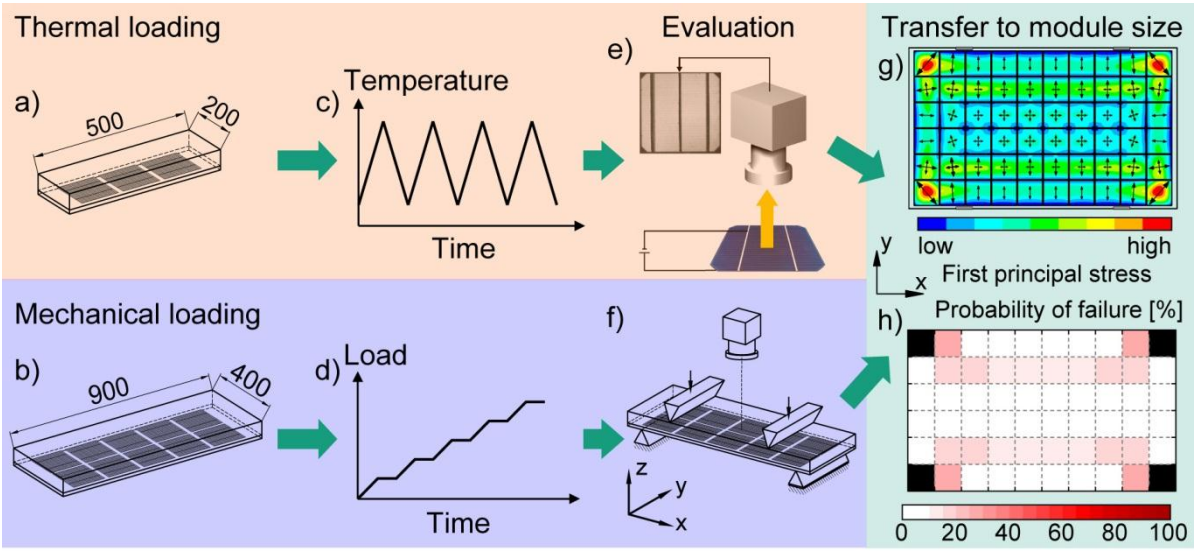

Figure 1: Experimental approach for separate investigation of thermal and mechanical loading.

2 EXPERIMENTAL APPROACH

To investigate cracks in encapsulated solar cells systematically, an approach is chosen, that considers thermal and mechanical loading separately by using adapted test specimens on smaller scales (mini-modules).

Figure 1 shows schematically the experimental approach and the used specimen layouts.

2.1 Test specimens

Because thermal and mechanical loading shall be investigated separately, mini-module layouts have been set up. The layouts and the dimensions were optimized to fit the requirements of the individual experimental setups by using finite element analysis (FEA). The dimensions of the test specimens are depicted in Figure 1a and b.

The mini-modules are produced using laboratory equipment but process parameters are selected preferably similar to the industrial processes. In previous publications test specimens with hand soldered solar cells were investigated [2, 10]. In this work industrially soldered cell strings were used. The cells have standard dimensions (156 mm; full-square; back surface field; 3 busbars). The test specimens are unframed and consist of a 4 mm glass pane, EVA encapsulant and a polymeric backsheet. The influence of varied specimen layouts is analyzed in [11]. In this work the influence of different cells and different manufacturing procedures is investigated. Some of the specimens have been produced at the Fraunhofer CSP using a laminator on laboratory scale and soldered cells from Q-Cells. Other specimens were produced completely by Q-Cells. Table I gives an overview over the test specimens.

For thermal loading the mini-modules consist of three solar cells that are connected in series.

For mechanical loading the mini-modules consist of 10 cells that are arranged depending on the loading direction (see Section 2.2).

2.2 Test procedure and test conditions

The test procedure is depicted schematically in Figure 1c to f. The test specimens were analyzed after each manufacturing step and after defined load steps using qualitative electroluminescence imaging.

For thermal loading the mini-modules are exposed to a thermal cycling process according to IEC 61215 (-40°C, +85°C) and were analyzed after 50, 100 and 200 cycles (Figure 1c). After thermal loading EL images at the specified analysis points are available.

The mechanical loading was performed at room temperature. The mini-modules are loaded in a 4-point bending setup, which induces a uniaxial bending at the encapsulated cells (Figure 1f). The used test setup is described in more detail in [11]. The crack occurrences in the cells can be investigated with respect to the loading direction. Therefore it was differentiated whether the bending was induced parallel or perpendicular to the busbars of the cells. For this purpose two different mini-module layouts have been defined. If the mini-module consists of two cell strings with five cells each, which have their busbars perpendicular to the bending rolls, the setup is called perpendicular. Otherwise if the cells are turned by 90°, i.e. the mini-module consists of five cell strings with two cells each, the setup is called parallel.

The load is increased stepwise and after the experiment load displacement data and EL images after each load step are available (Figure 1d).

2.3 Evaluation

The EL images are evaluated manually. Reliable crack identification and assessment is possible if images are compared before and after loading. If a crack propagates, its origin can be identified and analyzed in the previous steps.

Because silicon is a brittle material at room temperature cracks occur suddenly and catastrophic under tensile load. The origin of the fracture is one particular defect such as microscopic cracks, inclusions or dislocations. The size as well as the location of those defects is statistically distributed. As a consequence, the macroscopic fracture stress follows this distribution and leads to a large scatter of the strength values for each specimen. Because of this scatter a statistical evaluation is necessary.

After thermal loading visible cracks have been counted and a percentage of cells having existing cracks in the specimens is calculated. Also the length of the cracks is measured to detect if cracks grow from one step to another.

For mechanical loading the stress values in the silicon are calculated on the basis of a finite element analysis. The fracture stress is calculated by considering the measured force at which a crack was observed and the position of the crack origin in the cells. All fracture stress values from one specimen type are evaluated by using the Weibull

Table I: Overview over tested mini-modules.

Test specimen name	Cell type	Cell thickness [µm]	Number of specimens (Number of tested cells)	Manufacturer	Test setup
M, QC, 180 µm, 0°	Multi-crystalline	180	1 (6)	Q-Cells	Mechanical load, perpendicular
M, QC, 180 µm, 90°	Multi-crystalline	180	3 (18)	Q-Cells	Mechanical load, parallel
M, QC, 130 µm, 0°	Multi-crystalline	130	4 (24)	Q-Cells	Mechanical load, perpendicular
M, CSP, multi, 0°	Multi-crystalline	180	2 (12)	Fraunhofer CSP	Mechanical load, perpendicular
M, CSP, multi, 90°	Multi-crystalline	180	2 (12)	Fraunhofer CSP	Mechanical load, parallel
M, CSP, mono, 0°	Mono-crystalline	180	4 (12)	Fraunhofer CSP	Mechanical load, perpendicular
M, CSP, mono, 90°	Mono-crystalline	180	2 (12)	Fraunhofer CSP	Mechanical load, parallel
M, CSP, mono, 0°, TCT	Mono-crystalline	180	6 (36)	Fraunhofer CSP	Mechanical load, perpendicular, after thermal cycling
T, CSP, mono, 0°	Mono-crystalline	180	5 (15)	Fraunhofer CSP	Thermal cycling
T, CSP, multi, 0°	Multi-crystalline	180	5 (15)	Fraunhofer CSP	Thermal cycling

distribution function, which is typically used for silicon [12]. Every data point in the Weibull plots represents the fracture stress of one crack occurrence. Two characteristic parameters are determined by a Weibull evaluation, the characteristic strength σ_θ and the Weibull modulus m as a measure for the scattering. The probability of failure P_f represents the probability that a specimen breaks at a specific stress σ. The characteristic strength σ_θ represents the stress for a probability of failure of 63.2 %.

$$P_f(\sigma) = 1 - e^{-\left(\frac{\sigma}{\sigma_\theta}\right)^m}$$

The higher the characteristic strength value for one specific cell type, the lower is the probability that the cells will break at a specific stress level. If the Weibull modulus m is higher, the scattering of the fracture stress values is lower, indicating higher reliability at equal strength.

3 RESULTS AND DISCUSSION

3.1 Cracks after mechanical loading

Figure 2 shows the EL images of two test specimens in the area between the load rolls after the last load step of the mechanical loading procedure. It has been found that cracks typically start at the busbars of the cells. The comparison between the cracks in the perpendicular setup (Figure 2a) with the cracks in the parallel setup (Figure 2b) shows significant differences. The perpendicular loading generates cracks, which run perpendicular to the busbars and show typically dendritic crack paths [9]. The cracks generated by the parallel loading have crack paths, which lie parallel to the busbars and produce electrically isolated cell areas. If the isolated cell area has no contact to the busbars, it appears completely dark in the EL image. If the load is removed most of the isolated cell parts are in contact again (not shown here). Similar observations have been shown by Gabor et al. [1]. It is expected that isolated cell areas occur in PV modules in the field, too, for example during snow load in the winter and are in contact again, when the module is unloaded again.

If cells have initial cracks prior to the mechanical loading procedure, they act predominantly as starting points for crack growth during mechanical loading. Those initial cracks might have occurred during production due to thermal loading during soldering or lamination. These cracks shall be discussed in more detail in Section 3.2.

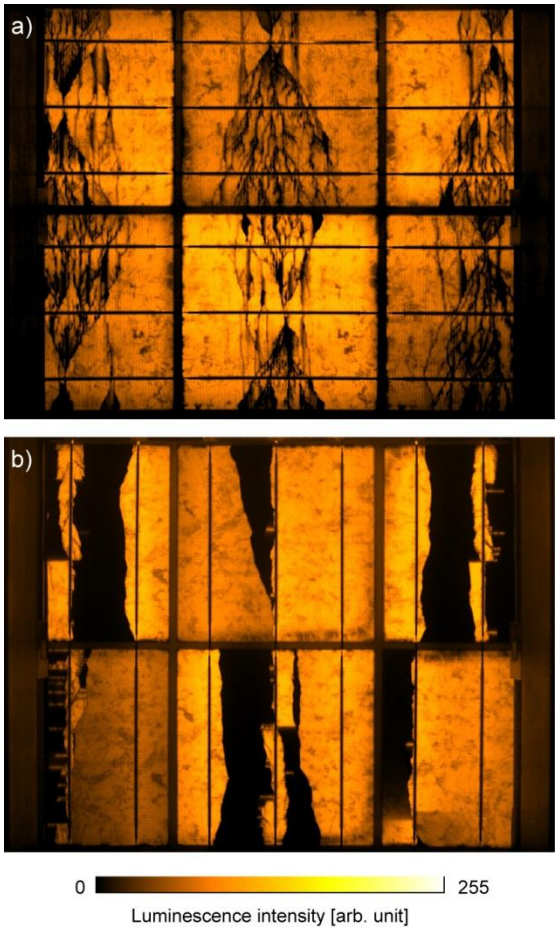

Figure 2: Electroluminescence image of the middle cells of test specimens including multi-crystalline cells during 4-point bending; (a) M, QC, 180 µm, 0°, perpendicular to the busbars; (b) M, QC, 180 µm, 90°, parallel to the busbars (displayed in false color representation).

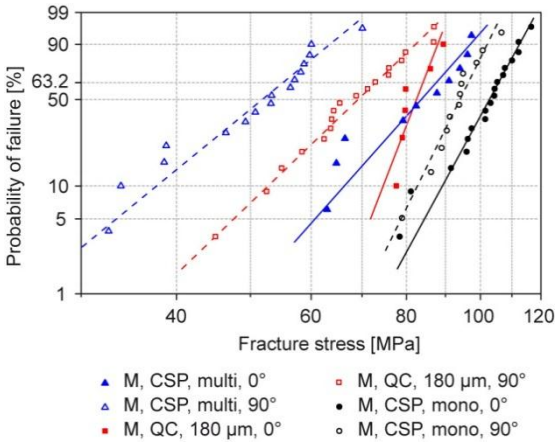

Figure 3: Weibull plot of the crack occurences in standard test specimens including multi-crystalline and mono-crystalline cells with a thickness of 180 µm.

Table II: Investigated Weibull distribution values according to Figure 5 (values for 95% confidence interval in brackets).

	σ_θ [MPa]	m [-]
M, QC, 180 µm, 0°	84.1 (79.7…88.5)	18.8 (9.3…31.8)
M, QC, 180 µm, 90°	72.9 (67.6…78.4)	6.9 (4.7…9.7)
M, QC, 130 µm, 0°	92.1 (87.3…96.9)	9.0 (6.2…12.4)
M, CSP, multi, 0°	87.6 (79.7…95.5)	8.1 (4.6…13.1)
M, CSP, multi, 90°	55.2 (50.1…60.4)	5.9 (3.8…8.4)
M, CSP, mono, 0°	105.7 (101.6…109.7)	13.3 (8.8…18.7)
M, CSP, mono, 90°	96.4 (92.2…100.6)	14.7 (9.1…21.3)

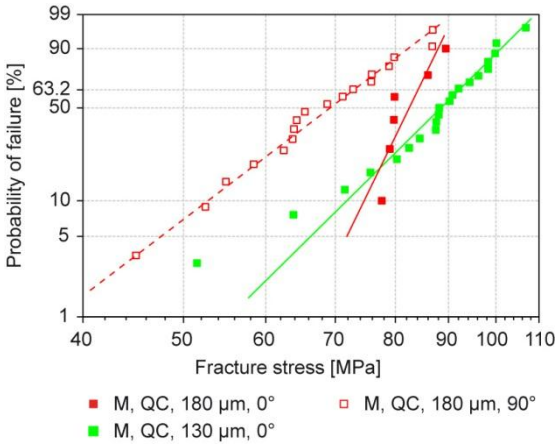

Figure 4: Weibull plot of crack occurences in standard test specimens including multi crystalline cells with variable thickness.

The fracture stress of the cells showing no initial cracks is evaluated by adapting a Weibull distribution as shown in Figure 3 and Figure 4. An evaluation that considers also the cells that include initial cracks is shown in [11]. The characteristic strength and the Weibull modulus are listed in Table II.

In Figure 5 it is obvious that the multi-crystalline cells show lower characteristic strength values than the mono-crystalline cells. For every cell type a difference between the perpendicular (filled dots) and the parallel loading direction (unfilled dots) could be observed.

The comparison between the laminates produced by Q-Cells and the Fraunhofer CSP shows differences in the strength values, especially for the loading parallel to the busbars. The reason for this might be different lamination process parameters and different material properties of the encapsulant.

Cells with varied thicknesses have been compared in Figure 4. They were all produced by Q-Cells and for the 130 µm cells only the perpendicular layout was tested. For the 180 µm cells in the perpendicular layout only one test specimen was available, so the Weibull distribution bases only on six data points from the six broken cells. For such a small data basis the uncertainty for the determination of the characteristic strength and the Weibull modulus is very high, so the results have to be interpreted carefully.

In the laminate the 130 µm cells show fracture at lower load magnitudes than the 180 µm cells, but from the Weibull plot and the confidence intervals one can see, that the characteristic strength differs not significantly, indicating an equal defect class and defect size. The finite element analysis proves that in the laminate the 130 µm cells are exposed to an approximately 20 % higher tension stress than the 180 µm cells for the same load magnitude.

To investigate the influence of the cracks on the electrical performance of the cells the power output of the specimens (M, QC, 180 µm) was measured under standard test conditions (STC) before and after new cracks have occurred. Therefore the test specimen was removed from the test setup and was placed in a module flasher.

The measured power output corresponds to the entire six cells in the middle of the test specimen. The relative

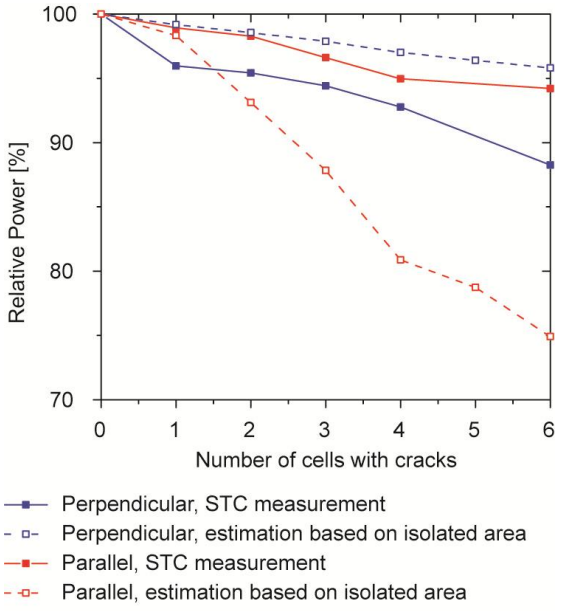

Figure 5: Relative power output of test specimens with cell cracks (power corresponds to total power of the six cells in the middle of the test specimen).

power of the specimen with broken cells is shown in Figure 5 (solid lines). The number of broken cells represents the load steps at which the test specimen was removed from the mechanical load test and was measured under STC. Because in both test specimens the last two cells broke one after the other during one load step the power output could not be measured for five broken cells.

As described earlier most of the isolated cell parts are in contact again if the load is removed from the specimen. Thus, the power of the specimens is always measured in a situation, where previously isolated cell parts are in contact again. Therefore the power loss is not related to the areas, which are not in contact during the loading.

In other publications it has been found that further temperature cycles and high humidity can cause permanent isolation of the crack faces [6]. This is causing a significant power loss of the modules.

To estimate the maximum power loss, which is caused by cell cracks, the isolated cell areas are measured manually from the EL images in Figure 2 by using a graphical evaluation tool (Figure 5, dashed lines).

It is obvious that the cracks parallel to the busbars generate higher power loss than cracks perpendicular to the busbars if the isolated area is considered under load. After a crack occurrence parallel to the busbars (red lines) the size of the isolated area per cell was found to be 25 % on average resulting in a remaining power output of approximately 75 % for the test specimen, when all cells show cracks. The measured power loss (STC) of the unloaded test specimen was found to be approximately 6 % resulting in a remaining power output of approximately 94 %.

For the cracks perpendicular to the busbars (blue lines) the isolated area per cell (average 4 %) is lower than the measured power loss (average 12 %). This indicates that here additional power is lost due to recombination at the excessive number of crack path surfaces.

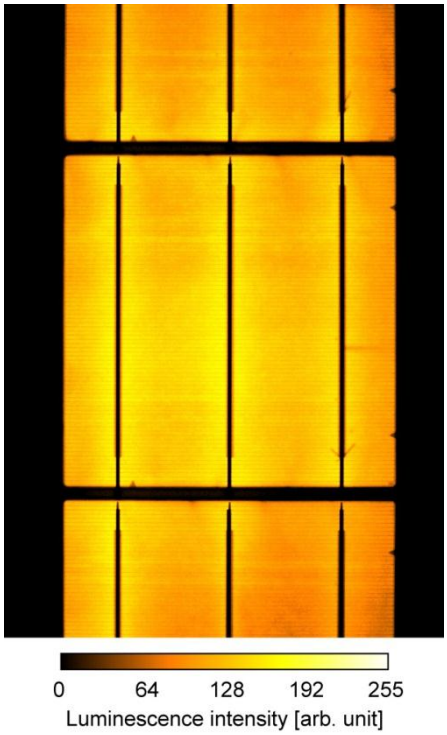

Figure 6: Electroluminescence image of a representative mono-crystalline cell in a test specimen after lamination (displayed in false color representation).

3.2 Cracks after thermal loading

Figure 6 shows a detail of a representative test specimen including three mono-crystalline cells with several visible cracks after lamination originating mainly at the busbars. Similar effects have been observed for multi-crystalline cells. Most of the cracks occurred after lamination at the side where the interconnecting ribbon changes from the front side of one cell to the back side of the next cell. Here, the soldered string with the individual cells has to withstand the mechanical pressure and the different expansion of the individual components during temperature change from lamination temperature to room temperature.

The test specimens were exposed to thermal cycling and the cracks were analyzed manually by using electroluminescence. For the investigated test specimens no visible crack growth and no newly occurred cracks could be observed. Different results have been found in other investigations for hand soldered cells [3, 10].

To investigate the effects during thermal loading in more detail, undamaged test specimens for the mechanical load test (Figure 1b) were exposed to different numbers of thermo cycles (Figure 1c) and were tested afterwards mechanically (Figure 1f). For this experiment mono-crystalline cells have been used (M, CSP, mono, 0°, TCT).

The results are shown in Figure 7 and Figure 8. It is obvious that the specimens after thermal cycling show significantly reduced strength values. So it is assumed that microscopic cracks have occurred or have propagated during thermal cycling, which act as starting points for cell breakage during mechanical loading.

The characteristic strength is decreased to approximately 50 % of the initial value after 200 thermo

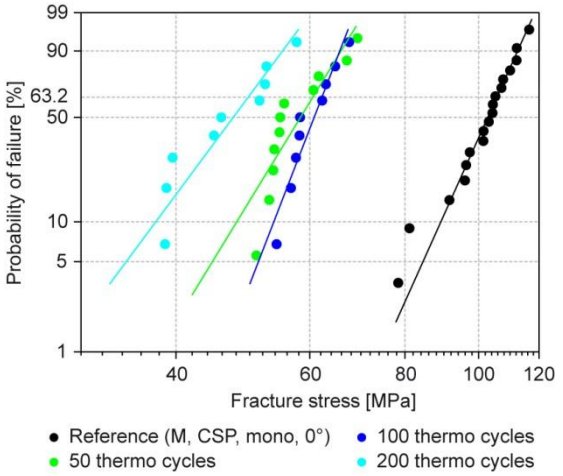

Figure 7: Weibull plot of crack occurrences in standard test specimens including mono crystalline cells (M, CSP, mono, 0°, TCT) after different number of thermo cycles.

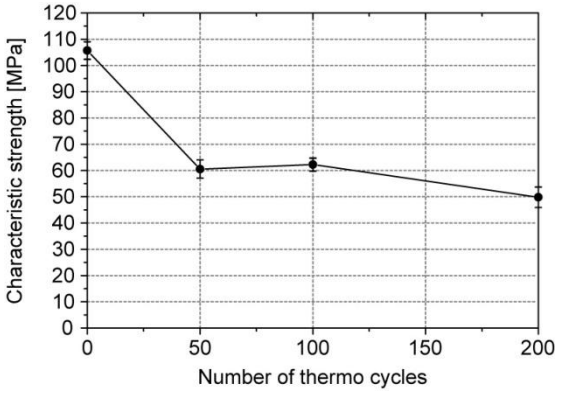

Figure 8: Characteristic strength of mono crystalline cells in standard test specimens plotted for different number of thermo cycles.

cycles. The main development of the cracks seems to occur at the first 50 thermo cycles. Similar effects have been observed for multi-crystalline cells (not shown here).

3.3 Transfer to full-scale modules

To transfer the results to full-scale PV modules, one has to analyze the stress distribution in a standard PV module with a clamped aluminum frame. Because of the boundary conditions the stress distribution is complex and cannot be calculated analytically. To solve this problem a finite element simulation was set up including all relevant materials and layers [11]. Figure 1g shows the result of the finite element analysis of a standard PV module under a uniform area load of 5.4 kPa. Additionally, the representative direction for the first and the second principal stress for each cell are depicted by arrows. The arrow size represents the stress magnitude. It is obvious that most of the cells show a biaxial stress distribution and first and second principal stress are aligned in x- and y-direction. In particular the four cells in the corners of the module show a 45° stress direction and the highest stress magnitude. With this information the varying distribution and orientation of cell cracks on different positions in full-scale PV modules which are described by Kajari-Schröder et al. [9] can be explained qualitatively.

The cells in the outer rows show an approximate uniaxial stress distribution and the expected crack directions are perpendicular to the busbars for the cells at the short edge and parallel to the busbars for the cells at the long edge of the PV module.

Many cells in the middle of the modul show a biaxial stress distribution and first and second principal stress have approximately the same magnitude. Here the finding is that the risk for cracks is much higher for cracks parallel to the busbars than perpendicular leads to the conclusion that for these cells more cracks parallel to the busbars will occur than perpendicular.

The finding that thermal loads lead to reduced fracture strength might be an explanation for the complete cracking of cells in full-scale PV modules during thermal cycling according to IEC 61215. If the fracture strength is reduced significantly already small loads can lead to cell breakage. Such small loads can arise during handling or due to the air circulation in the climate chamber.

If the simulated stress distribution in the PV module is evaluated with the statistically determined fracture strength values, a fracture probability per cell can be calculated for specific cell fracture strengths (Figure 1h) [11]. The probability of failure is dominated by the failure parallel to the busbars for these conditions, so more cracks parallel to the busbars are expected to occur under mechanical load, thus generating larger isolated cell areas. It might be promising to influence the stress direction inside the cells in that way that it is aligned with the direction of the busbars. This can be done for example by changing the mounting of the module [13].

4 CONCLUSIONS AND OUTLOOK

In this work a new approach was applied to systematically investigate crack formation and crack growth in encapsulated solar cells. By using the experimental setup influences of thermal and mechanical loading on cracks in encapsulated crystalline solar cells could be analyzed under well-known boundary conditions and the observed mechanisms could be transferred qualitatively to full-scale PV modules. Furthermore the presented experimental setup was used to investigate the influence of variable cell thickness and of occurring effects during thermal cycling.

An overview of statistical fracture strength distributions has been shown for different cell types and different manufacturers.

The characteristic fracture strength of a batch of cells with a thickness of 130 µm was found to be in the same range as of comparable cells with a thickness of 180 µm.

The power loss of the mini-modules with cracks was measured and it was discussed with respect to the crack orientation. Large isolated areas have been found to be caused by cracks parallel to the busbars. Additional power loss is assumed to be caused by surface recombination at the crack fronts, especially for dendritic cracks.

It was found that during thermal cycling the characteristic strength is reduced significantly, but no crack propagation could be observed by EL imaging. It was found that the main development of the damage occurs at the first 50 thermo cycles. This finding might be useful to decrease the testing effort for thermo cycle tests by reducing the required number of thermo cycles.

The gained findings on the mechanisms of crack development and crack growth in encapsulated solar cells can be transferred to full-scale PV modules and many effects that can be observed in the field can by explained qualitatively. With the knowledge of the fracture strength of the encapsulated cells a reliability concept can be set up, which can be used to optimize the module layout for reduced cell breakage [13].

ACKNOWLEDGEMENTS

This work was supported by the German Federal Ministry for Education and Research (BMBF) within the framework of the Leading-Edge Cluster Competition and Solarvalley Central Germany under contract no. 03SF0400A ("xµ-Module") that is gratefully acknowledged. In addition, the authors would like to thank the group Optical Materials and Spectroscopy at Fraunhofer CSP for their support on the test equipment, the team Polymeric Materials at Fraunhofer CSP for their support during specimen lamination and Frank Wenger and Sascha Lindig for their support in specimen preparation and execution of the tests.

REFERENCES

[1] A. Gabor, M. Ralli, S. Montminy, L. Alegria, C. Bordonaro, J. Woods, J. Felton, Proceedings 21st European Photovoltaic Solar Energy Conference, (2006) 2042-2047.
[2] M. Sander, S. Dietrich, M. Pander, S. Schweizer, M. Ebert, J. Bagdahn, Proceedings SPIE Optics and Photonics, 8112 (2011), 811209.
[3] M. Sander, B. Henke, S. Schweizer, S. Dietrich, M. Pander, M. Ebert, J. Bagdahn, Proceedings Symposium Photovoltaische Solarenergie (2011).
[4] T. Fuyuki, H. Kondo, T. Yamazaki, Y. Takahashi, Y. Uraoka, Applied Physics Letters, 86 (2005) 1-3.
[5] P. Grunow, P. Clemens, V. Hoffmann, B. Litzenburger, L. Podlowski, Proceedings 20th European Photovoltaic Solar Energy Conference, (2005) 2042-2047.
[6] M. Köntges, I. Kunze, S. Kajari-Schröder, X. Breitenmoser, B. Bjørneklett, Solar Energy Materials and Solar Cells 95 (2011), 1131-1137.
[7] S. Dietrich, M. Pander, M. Sander, S. H. Schulze, M. Ebert, Proceedings SPIE Optics and Photonics, 7773 (2010).
[8] M. Köntges, S. Kajari-Schröder, I. Kunze, U. Jahn, Proceedings 26th European Photovoltaic Solar Energy Conference, (2011) 3290-3294.
[9] S. Kajari-Schröder, I. Kunze, U. Eitner, M. Köntges, Solar Energy Materials and Solar Cells 95 (2011), 3054-3059.
[10] M. Sander, B. Henke, H. Schwarz, S. Dietrich, S. Schweizer, M. Ebert, J. Bagdahn, Proceedings SPIE Optics and Photonics, 7773 (2010).
[11] M. Sander, S. Dietrich, M. Pander, M. Ebert, J. Bagdahn, Solar Energy Materials and Solar Cells (2012), Submitted.
[12] R. B. Abernethy, The New Weibull Handbook, 4 (2005).
[13] S. Dietrich, M. Sander, M. Pander, M. Ebert, Proceedings SPIE Optics and Photonics, (2012), Submitted.